Catalysis Letters (2022) 152:2767–2778
https://doi.org/10.1007/s10562-021-03854-8

Epoxidation of Olefins with Molecular Oxygen Over Layered Double Hydroxide Catalyst in the Presence of Benzaldehyde

Yuwei Xin[1,2] · Ya Liu[1,2] · Hong-yu Zhang[1,2] · Yuecheng Zhang[1,3] · Jiquan Zhao[1,2]

Received: 15 July 2021 / Accepted: 2 November 2021 / Published online: 13 November 2021

Abstract

A Fe embedded MgAl layered double hydroxide ($MgAlFe_{0.4}$-LDH) showed excellent performances in the epoxidation of various olefins with O_2/benzaldehyde as oxidant at mild conditions. Under optimal conditions, the olefins including terminal aliphatic olefins, cyclohexene and styrene were all converted to the corresponding epoxides in conversions close to 100% and selectivity higher than 95%. The epoxidation is accomplished in two elementary steps, which are catalytic oxidation of benzaldehyde to peroxybenzoic acid, and epoxidation of olefin to epoxide by peroxybenzoic acid generated in situ. The catalyst also exhibited good stability and recyclability. The characterization results revealed that the Fe species are present in the state of Fe^{3+} fully incorporated into the Mg/Al-LDH layers, and act as active sites in the catalyst. The embedment of Fe into MgAl-LDH largely increased the surface area and pore volume of Mg/Al-LDH, which is another factor enhancing the activity of the catalyst.

Graphical Abstract

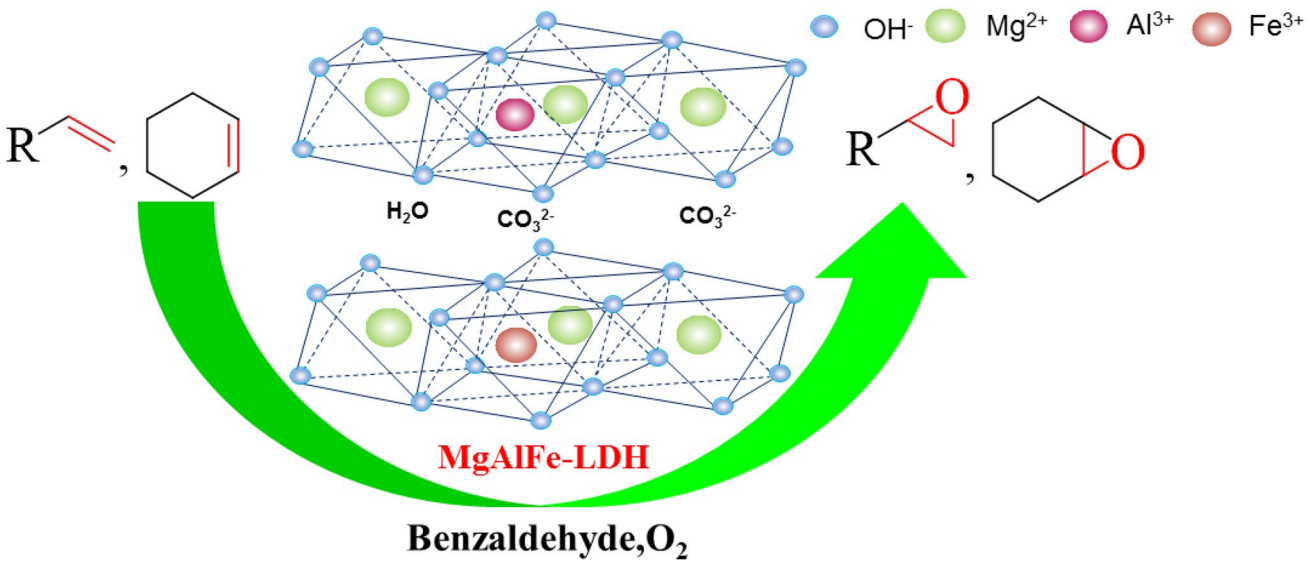

Keywords 1-hexene · Epoxidation · Layered double hydroxide · Oxygen · Hydrotalcite

✉ Yuecheng Zhang
yczhang@hebut.edu.cn

✉ Jiquan Zhao
zhaojq@hebut.edu.cn

[1] School of Chemical Engineering and Technology, Hebei University of Technology, Tianjin 300131, China

[2] Hebei Provincial Key Laboratory of Green Chemical Technology and High Efficient Energy Saving, Tianjin 300131, China

[3] National-Local Joint Engineering Laboratory for Energy Conservation of Chemical Process Integration and Resources Utilization, Hebei University of Technology, Tianjin 300130, China

1 Introduction

Olefin epoxidation is an important reaction of both academic and industrial interests, because epoxides can be ring-opened in many ways to construct complex organic structures [1]. For instances, epoxides as intermediates can be widely used in plastics, medicine, food and other production fields [2–4]. Traditional protocols for the manufacture of epoxides rely on the chlorohydrin process, catalytic or non-catalytic epoxidation processes with expensive organic peroxides and peracids [5], which suffer from disadvantages of low product selectivity, environmental pollution, unsafety, and high cost in some cases [6]. In contrast to the traditional non-green processes, the olefin epoxidation with H_2O_2, O_2 and TBHP as oxidants is of great advantage to the economy and environment due to the cheapness of the oxidants, and H_2O as a sole by-product in principle in the cases of H_2O_2, O_2 as oxidants, as well as high selectivity towards epoxides with TBHP as oxidant [7–9]. A variety of heterogeneous and homogeneous catalysts were developed for the H_2O_2-based epoxidation, and some of which have been applied to industrial production [1, 10]. Various catalysts were also explored for the epoxidation with O_2 as terminal oxidant [11–17]. Generally, the direct olefin epoxidation over heterogeneous catalysts with O_2 as oxidant suffers from the disadvantages of harsh reaction conditions and low olefin conversion or epoxide selectivity [18, 19]. Homogeneous or immobilized metal complexes showed good performances in the epoxidation with O_2 at ambient conditions in the presence of coreductants, but these catalysts have the drawbacks of complicated synthesis process, poor stability, and difficult recycling [15–17]. Therefore, it is still a challenge to develop stable, efficient and recyclable catalysts for olefin epoxidation with O_2.

It is noteworthy that Baeyer–Villiger oxidation reaction, which is commonly carried out with peracid oxidants, can proceed smoothly with O_2/benzaldehyde instead of peracid oxidants at low reaction temperatures over the layered double hydroxides (LDHs) based catalysts [20]. In these cases, benzaldehyde is firstly converted to peroxybenzoic acid by O_2 over the catalysts, then the in situ generated peroxybenzoic acid oxidizes ketones to esters. LDHs, also known as hydrotalcite compounds, are a kind of functional layered anionic clay materials with the general chemical composition $[M^{2+}_{1-x}M^{3+}_{x}(OH)_2]^{x+}[A^{n-}]_{x/n}\cdot mH_2O$ [21], where M^{2+} and M^{3+} are di- and trivalent metal cations, x represents the molar ratio of $M^{3+}/(M^{2+}+M^{3}+)$, and A^{n-} are the interlayer anions with charge *n*, which can be inorganic anions, organic anions, anionic complexes or biomolecules [22–24]. The LDHs-based catalysts could be readily obtained by embedment of metal species into the LDH layers, and showed good catalysis in various reactions [25–27]. However, the LDHs-based catalysts were not very effective in the aerobic epoxidation of olefins due to their low epoxide selectivity in the absence of coreductants [28–31].

Inspired by the excellent results of Baeyer–Villiger oxidation reaction with O_2/benzaldehyde over LDHs-based catalysts, herein, several LDHs-based catalysts were prepared by embedment of Ni, Cu, Zn, Co, Mn and Fe into MgAl hydrotalcite laminate by co-precipitation method, respectively. The catalysts were evaluated in the olefin epoxidation with O_2/benzaldehyde, and a catalyst $MgAlFe_{0.4}$-LDH was found to be excellent in the reaction.

2 Experimental

2.1 Catalyst Preparation

All reagents were analytical grade and used as received without further purification. Metal salts and reagents for catalyst preparation were purchased from Tianjin Keruisi Chemical Reagent Cooperation. Solvents were provided by Tianjin Hengshan Chemical Technology Cooperation. Olefins were purchased from Chemart (Tianjin) Chemical Technology Cooperation.

2.1.1 Preparation of Neat MgAl-LDH

Neat MgAl-LDH was prepared according the procedure in literature [32]. For instance, 7.69 g (0.03 mol) of $Mg(NO_3)_2\cdot 6H_2O$ and 3.75 g (0.01 mol) of $Al(NO_3)_3\cdot 9H_2O$ were dissolved in 50 mL of deionized water in a four-necked round bottom flask equipped with mechanical stirring, thermometer and dropping funnel. An alkaline solution was prepared by dissolving 3.18 g (0.03 mol) of Na_2CO_3 and 2.80 g (0.07 mol) NaOH in 60 mL of deionized water. Under strong agitation, the alkaline solution was added in dropwise into the salt solution through the dropping funnel in about 1.5 h. The resulting mixture was heated at 68 ℃ for 12 h with agitation. Then the slurry was cooled to room temperature and filtered to afford a white power. The white power was washed with a plenty of water and dried at 110 ℃ for 12 h, which was denoted as MgAl-LDH.

2.1.2 Preparation of $MgAlM_{0.3}$-LDH (M = Ni, Fe, Cu, Zn, Co or Mn; 0.3 is the M to Mg Molar Ratio)

For the preparation of $MgAlNi_{0.3}$-LDH, 0.87 g (0.003 mol) of $Ni(NO_3)_2\cdot 6H_2O$, 7.69 g (0.03 mol) of $Mg(NO_3)_2\cdot 6H_2O$ and 3.75 g (0.01 mol) of $Al(NO_3)_3\cdot 9H_2O$ were dissolved in 50 mL of deionized water to give a salt solution. To this salt solution was added in dropwise an alkaline solution

prepared by dissolving 3.18 g (0.03 mol) of Na_2CO_3 and 2.80 g (0.07 mol) NaOH in 60 mL of deionized water under strong agitation in about 1.5 h. The rest of procedures was same as those for preparing neat MgAl-LDH. Finally, a light green powder was obtained, which was denoted as $MgAlNi_{0.3}$-LDH.

By replacing $Ni(NO_3)_2{\cdot}6H_2O$ with same moles of $Fe(NO_3)_3{\cdot}9H_2O$, $CuSO_4{\cdot}5H_2O$, $Zn(NO_3)_2{\cdot}6H_2O$, $CoSO_4{\cdot}7H_2O$, and $MnSO_4{\cdot}H_2O$, the corresponding catalysts $MgAlFe_{0.3}$-LDH (light yellow powder), $MgAlCu_{0.3}$-LDH (light blue powder), $MgAlZn_{0.3}$-LDH (white powder), $MgAlCo_{0.3}$-LDH (light purple powder), and $MgAlMn_{0.3}$-LDH(light yellow powder) were obtained, respectively.

2.1.3 Preparation of $MgAlFe_x$-LDH

According to the above procedures, several catalysts $MgAlFe_x$-LDH with different Fe contents (x = 0.1, 0.2, 0.3, 0.4 and 0.5) were obtained, where x stands for the molar ratios of Fe to Mg.

2.1.4 Preparation of Trivalent Co Catalyst $MgAlCo_{0.3}$-LDH-1

The trivalent Co catalyst was prepared according the procedure in literature [33] in the material compositions of $Co(NO_3)_2{\cdot}6H_2O$ 0.87 g (0.003 mol), $Mg(NO_3)_2{\cdot}6H_2O$ 7.69 g (0.03 mol) and $Al(NO_3)_3{\cdot}9H_2O$ 3.75 g (0.01 mol). The pink power was denoted as $MgAlCo_{0.3}$-LDH-1.

2.1.5 Preparation of Trivalent Mn Catalyst $MgAlMn_{0.3}$-LDH-1

The trivalent Mn catalyst was prepared according the above procedure for preparing $MgAlMn_{0.3}$-LDH just by replacing $MnSO_4{\cdot}H_2O$ with same moles of $Mn(CH_3COO)_3{\cdot}2H_2O$. A dark brown power was obtained, which was denoted as $MgAlMn_{0.3}$-LDH-1.

2.2 Characterization of Catalysts

The X-ray diffraction (XRD) patterns of the catalyst samples were taken on a Bruker D8 X-ray diffractometer with Ni-filtered Cu Kα radiation (150 mA, 40 kV) in the 2θ range of 5°-90°. Fourier transform infrared (FT-IR) spectra were recorded with a Bruker Vector22 FT-IR instrument. N_2 adsorption–desorption analysis was carried out on a Micromeritics ASAP 2460, from which the surface areas, total pore volumes and pore size distributions of the samples were achieved. The scanning electron microscope (SEM) images were taken on a Quanta 4500 FEG instrument. The spectra of X-ray photoelectron spectroscopy (XPS) was recorded using an ESCALab 250Xi spectrometer with monochromatic Al Kα radiation. The ICP analysis was taken on a T.J.A. ICP-9000(N + M) type ICP-AES instrument.

2.3 Catalytic Test

In a typical process, benzaldehyde (24 mmol), 1,2-dichloroethane (40 mL), and catalyst (0.05 g) were added into a flask successively. The reaction mixture was stirred at 45 °C, and pure oxygen was bubbled into the reaction mixture at a rate of 10 mL/min under atmospheric pressure. After a period of time (induction period), olefin (8 mmol) was added in dropwise into the reaction mixture, and the resulted mixture was stirred at the same temperature until reaction completion. The reaction was monitored by GC equipped with a InterCap 624 capillary column (d_f = 30 μm, 0.53 mm × 30 m) and a FID detector.

2.3.1 Warning

Electrostatic sparks caused by static or metal collision are strictly prohibited to avoid explosion due to the presence of oxygen throughout the process.

2.4 Product Analysis

Reaction mixture was analyzed by a Shimadzu GC-2018 gas chromatography equipped with a InterCap 624 capillary column (d_f = 30 μm, 0.53 mm × 30 m). The GC temperature program was set to 60 °C for 1 min and 20 °C/min up to 250 °C with retention time of 15 min. The olefin conversion and epoxide selectivity were calculated according to the following equations:

$$\text{Conversion}\ (\%) = \frac{\text{Moles of reacted olefin}}{\text{Moles of initial olefin}} \times 100\%$$

$$\text{Selectivity}(\%) = \frac{\text{Moles of epoxide}}{\text{Moles of all oxidation products}} \times 100\%$$

3 Results and Discussion

3.1 Catalyst Characterization

Figure 1A shows the XRD patterns of the catalysts embedded with different metals. All the XRD patterns exhibit diffraction peaks at *2θ* of 11°, 23°, 34°, 39°, 47°, 61° and 62°, respectively, corresponding to the characteristic crystal planes of hydrotalcite (003), (006), (009), (015), (018), (110) and (113) [34, 35], which are indicative of the characteristics of hydrotalcite-like structures. The symmetrical and clear diffraction peaks appeared at the (110) and (113)

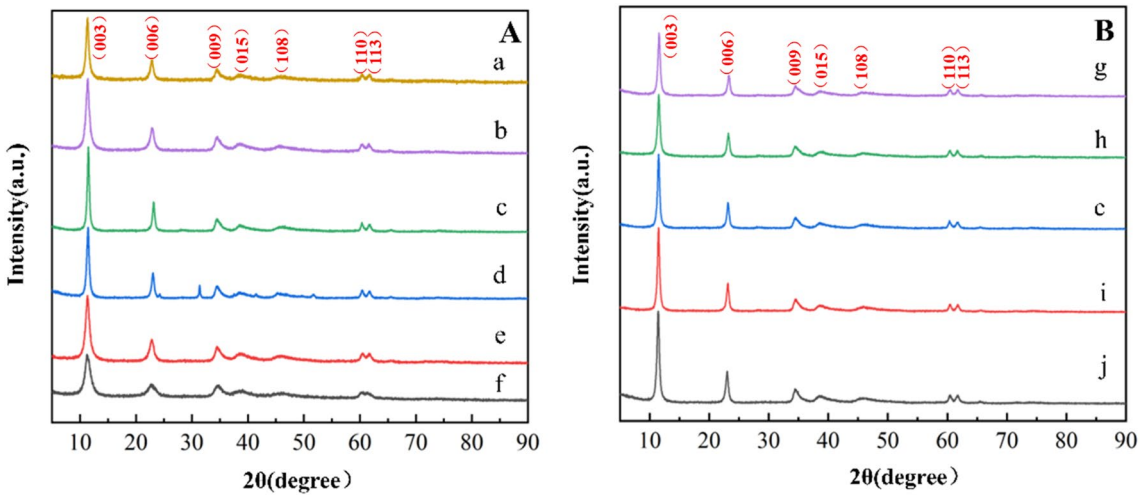

Fig. 1 XRD patterns of different LDH catalysts (*a*) $MgAlCo_{0.3}$-LDH, (*b*) $MgAlCu_{0.3}$-LDH, (*c*) $MgAlFe_{0.3}$-LDH, (*d*) $MgAlMn_{0.3}$-LDH, (*e*) $MgAlNi_{0.3}$-LDH, (*f*) $MgAlZn_{0.3}$-LDH, (*g*) $MgAlFe_{0.5}$-LDH, (*h*) $MgAlFe_{0.4}$-LDH, (*i*) $MgAlFe_{0.2}$-LDH, (*j*) $MgAlFe_{0.1}$-LDH

crystal planes, indicating regular structure, good symmetry and high crystallinity of the catalysts. The relatively low peak intensities of the XRD pattern of $MgAlZn_{0.3}$-LDH indicated the low crystallinity and order of the layered structure. In the XRD pattern of $MgAlMn_{0.3}$-LDH, some weak peaks at 2θ of 24°, 31°, 42° and 52° are found besides the characteristic peaks of hydrotalcite, which are attributed to rhodochrosite $MnCO_3$ [36], suggesting the presence of $MnCO_3$ as impurity in catalyst $MgAlMn_{0.3}$-LDH. Except for that of $MgAlMn_{0.3}$-LDH, no additional peaks originating from crystalline metal species are observed from the XRD patterns of the other catalysts, indicating a high dispersion of embedded metal on the supports.

As shown in Fig. 1B, the XRD patterns of the catalysts embedded with different amount of Fe all exhibit sharp, strong peaks for the (003) and (006) planes at low *2θ* angles, as well as weaker and symmetrical peaks for the (110) and (113) planes at higher angle, indicating also the formation crystalline hydrotalcite-like structures. Moreover, no Fe^{3+} related phases are observed in the XRD patterns of all the Fe embedded MgAl-LDH catalysts, indicating the good dispersion and embedment of Fe^{3+} ions in the framework of Mg/Al-LDH.

Figure 2 shows the FT-IR spectra of the samples of neat MgAl-LDH and metal embedded catalysts. As shown in Fig. 2, all the samples exhibit a wide and strong band around 3500 cm^{-1}, which is attributed to the stretching vibration of

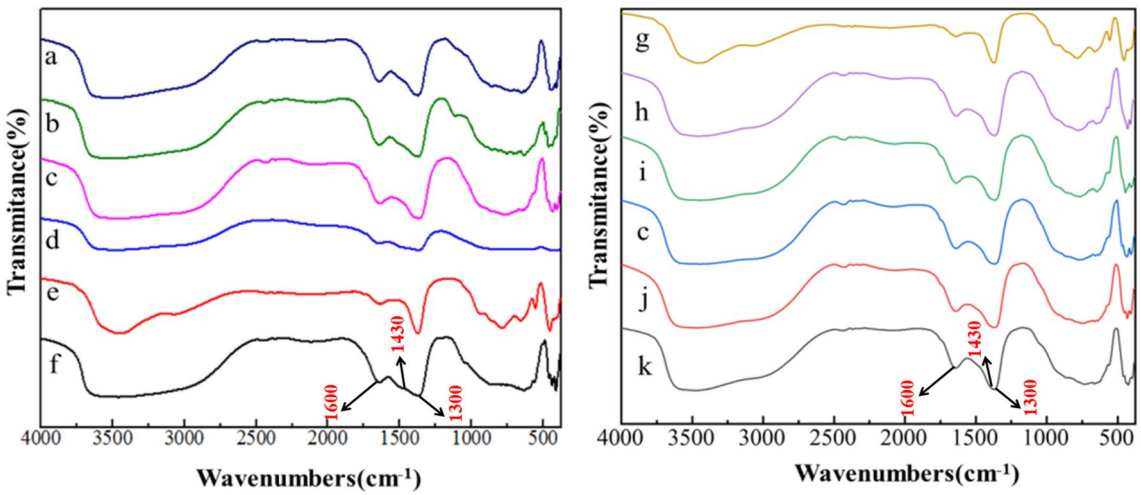

Fig. 2 FT-IR spectra of different catalysts (*a*) $MgAlCo_{0.3}$-LDH, (*b*) $MgAlCu_{0.3}$-LDH, (*c*) $MgAlFe_{0.3}$-LDH, (*d*) $MgAlMn_{0.3}$-LDH, (*e*) $MgAlNi_{0.3}$-LDH, (*f*) $MgAlZn_{0.3}$-LDH, (*g*) MgAl-LDH, (*h*) $MgAlFe_{0.5}$-LDH, (*i*) $MgAlFe_{0.4}$-LDH, (*j*) $MgAlFe_{0.2}$-LDH, (*k*) $MgAlFe_{0.1}$-LDH

hydroxyl groups from the interlayer water molecules, and existence of hydrogen bonds with a wide range of strength [37, 38]. The broad, very weak shoulder close to 3000 cm^{-1} is originating from the hydrogen bonding of interlayer water molecules to interlayer carbonate anions (CO_3^{2-}) [35, 38]. The absorption peak near 1600 cm^{-1} is attributed to the bending mode of interlayer water molecules [39, 40]. The sharp and intense peak near 1300 cm^{-1} is due to the mode ν_3 of the interlayer carbonate species [40, 41]. Its existence indicates that the hydrotalcite-like catalyst with interlayer anion CO_3^{2-} was successfully synthesized, and this peak shifts to a lower wavenumber compared with the absorption peak of free C-O in CO_3^{2-} at 1430 cm^{-1}, also indicating the strong hydrogen bonding interaction between the interlayer anions CO_3^{2-} and H_2O. The absorption peaks in the range of 400 to 800 cm^{-1} belong to the lattice vibration modes of M–O, O-M–O and M–O-M (M are the metals involved) [42].

Several $MgAlFe_x$-LDH (x = 0.1, 0.4, 0.5) catalysts were analyzed by XPS to elucidate the chemical states of metals on the surface of LDH. Figure 3A displays the XPS survey spectra of the three catalysts, whose peaks are mainly attributed to C 1 s, O 1 s, Mg 1 s, Al 2p, and Fe 2p. All the elements for constructing the $MgAlFe_x$-LDH catalysts are found in the spectra, which in combination with the XRD and FT-IR results, suggesting the successful synthesis of $MgAlFe_x$-LDH. In the Fe 2p spectra as shown in Fig. 3A, the main Fe $2p_{3/2}$ peak is around 711 eV, associated with a satellite peak at 719 eV, and the main Fe $2p_{1/2}$ peak is found around 724 eV [37, 43]. The appearance of the satellite peak near the main peak of Fe 2p is usually an indicator of Fe^{3+} valence state [44]. The results suggest that the Fe species in the $MgAlFe_x$-LDH catalysts exist in the state of Fe^{3+}.

Figure 4 shows the SEM images of $MgAlFe_x$-LDH catalysts. The three catalysts all show a similar morphology of a typical hydrotalcite structure of lamellar stack [44]. The embedment of Fe had no damage to the structure of hydrotalcite interlayer. The comprehensive XRD and FT-IR results indicated that the Fe embedded MgAl-LDH catalysts were successfully synthesized.

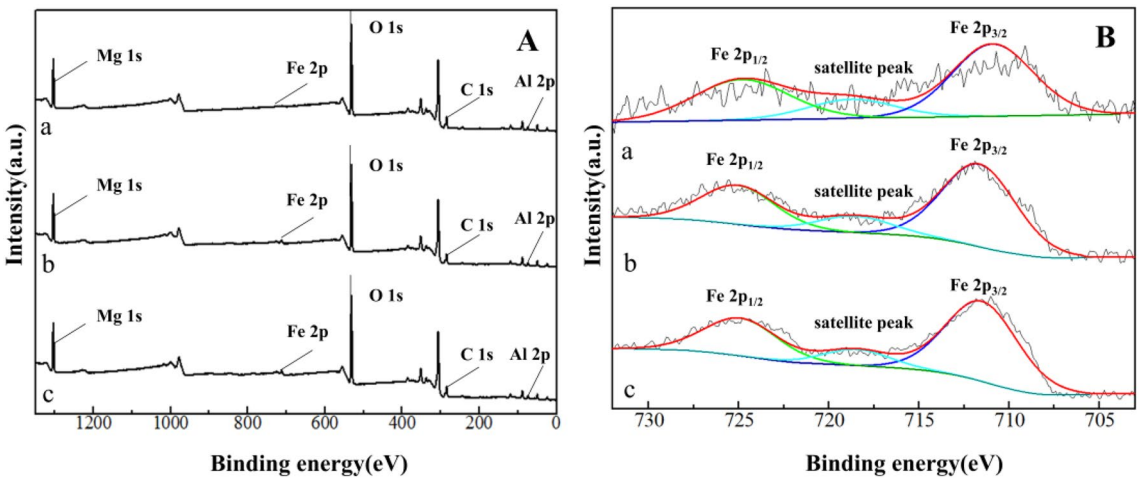

Fig. 3 The wide scan XPS spectra (**A**) and Fe 2p XPS spectra (**B**) of different catalysts (a) $MgAlFe_{0.1}$-LDH, (b) $MgAlFe_{0.4}$-LDH, (c) $MgAlFe_{0.5}$-LDH

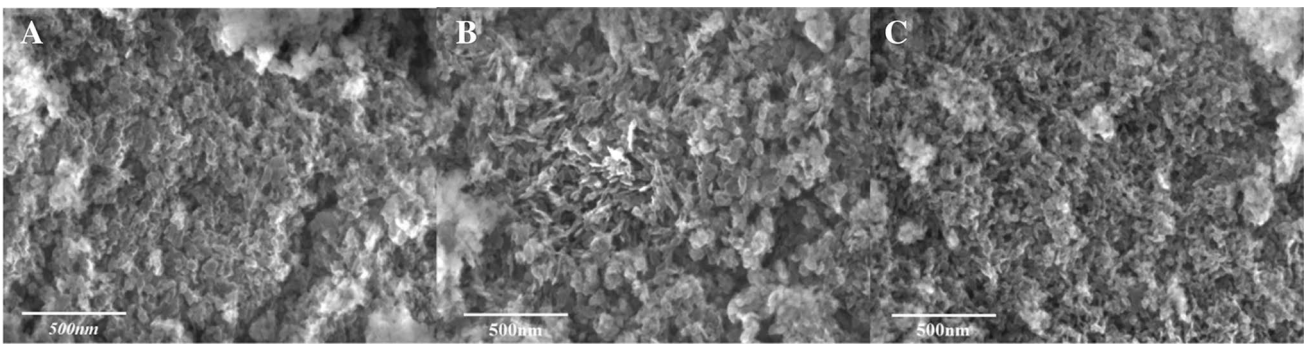

Fig. 4 SEM images of different catalysts **a** $MgAlFe_{0.1}$-LDH, **b** $MgAlFe_{0.4}$-LDH, **c** $MgAlFe_{0.5}$-LDH

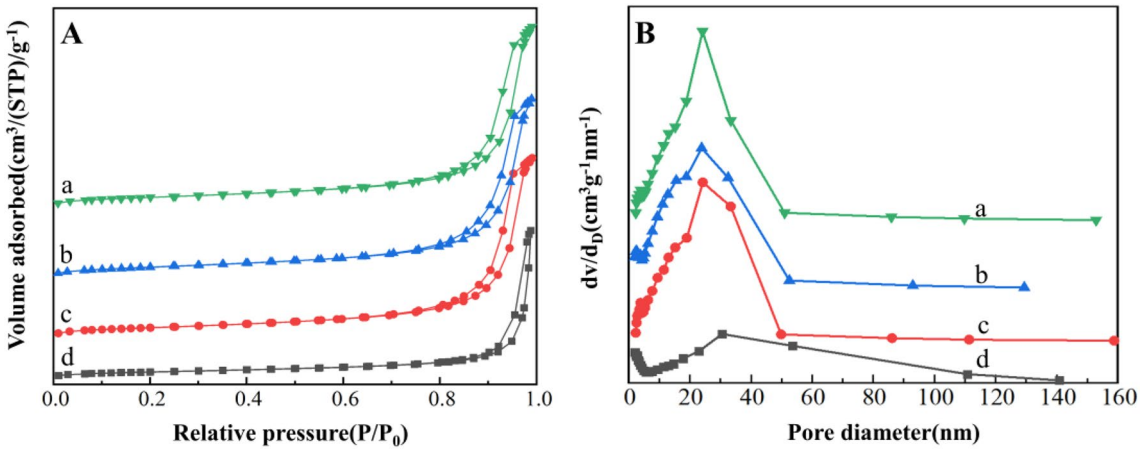

Fig. 5 N_2 adsorption–desorption isotherms **A** and distribution **B** of different catalysts (a) $MgAlFe_{0.5}$-LDH, (b) $MgAlFe_{0.4}$-LDH, (c) $MgAlFe_{0.1}$-LDH, (d) MgAl-LDH

Table 1 Specific area (BET-N_2), pore volume and pore size of different samples

Entry	Catalyst	Specific area[a] (m^2/g)	Pore volume[b] (cm^3/g)	Pore size[c] (nm)
1	MgAl-LDH	59	0.51	31
2	$MgAlFe_{0.1}$-LDH	97	0.63	22
3	$MgAlFe_{0.4}$-LDH	100	0.63	20
4	$MgAlFe_{0.5}$-LDH	98	0.63	22

[a]BET surface area

[b]BJH cumulative desorption pore volume

[c]Mean pore diameter = 4 V/S_{BET}

The N_2 adsorption–desorption analysis was performed to study the surface areas and porosity properties of $MgAlFe_x$-LDH catalysts with MgAl-LDH as reference sample. As shown in Fig. 5A, all the $MgAlFe_x$-LDH catalysts exhibit typical type IV isotherms with H3-type hysteresis loops same as that of MgAl-LDH, indicating the presence of a mesoporous structure [45]. This type of hysteresis loops appears at high P/P_0 region, which is commonly attributed to the accumulation of flake particles to form slit-shaped pores [46].

As exhibited in Fig. 5B, the catalysts possess mesopores with a relatively wide size distribution in the range of 20–40 nm. The specific surface areas, pore volumes and pore diameters of $MgAlFe_x$-LDH catalysts are summarized in Table 1. The results indicate that the introduction of iron into MgAl-LDH obviously increased the specific surface areas and pore volumes of the LDHs-based catalyst, which is favorable to mass transfer, thus improving the catalytic performances of the catalysts.

Table 2 The epoxidation of 1-hexene catalyzed by different LDHs-based catalysts

Entry	Catalyst[a]	Conv. (%)	Sel. (%)
1	MgAl-LDH	17	97
2	$MgAlNi_{0.3}$-LDH	18	98
3	$MgAlCu_{0.3}$-LDH	21	98
4	$MgAlFe_{0.3}$-LDH	90	99
5	$MgAlZn_{0.3}$-LDH	14	93
6	$MgAlCo_{0.3}$-LDH	48	88
6[a]	$MgAlCo_{0.3}$-LDH-1	85	90
7	$MgAlMn_{0.3}$-LDH	8	97
7[a]	$MgAlMn_{0.3}$-LDH-1	11	85

Reaction conditions: 1-hexene 8 mmol, benzaldehyde 24 mmol, catalyst 0.05 g, 1,2-dichloroethane 40 mL, O_2 10 mL/min, temperature 40 °C, induction time 3 h, reaction time 2.5 h

[a]$MgAlCo_{0.3}$-LDH-1 and $MgAlMn_{0.3}$-LDH-1 are the corresponding trivalent metal embedded catalysts

3.2 Screen of the Catalysts

It was reported that metal (Fe, Co, Ni or Cu) containing MgAl-LDH catalysts were active in the Baeyer–Villiger oxidation of ketones with O_2/benzaldehyde as oxidant [20, 32]. Therefore, several catalysts were initially prepared by embedding different bivalent metals (Ni, Cu, Fe, Zn, Co or Mn) into MgAl-LDH, and evaluated in the epoxidation of 1-hexene with O_2/benzaldehyde as oxidant. Besides, the trivalent Co and Mn embedded catalysts $MgAlCo^{III}_{0.3}$-LDH and $MgAlMn^{III}_{0.3}$-LDH were also prepared and evaluated in the same reaction. As shown in Table 2, the catalysts embedded with bivalent Ni, Cu, or Zn, almost showed same catalytic results as neat MgAl-LDH.

The trivalent Mn catalyst $MgAlMn_{0.3}$-LDH-1 showed slightly higher activity than its bivalent counterpart

$MgAlMn_{0.3}$-LDH, but still poorer activity than MgAl-LDH, which might be due to that Mn^{II} and Mn^{III} species was not the active sites in the oxidation reaction, but acted as an impurity leading to deterioration of the structure of $MgAlMn_{0.3}$-LDH. Both the bivalent and trivalent Co embedded catalysts $MgAlCo_{0.3}$-LDH and $MgAlCo_{0.3}$-LDH-1 exhibited higher activity than the neat MgAl-LDH, and $MgAlCo_{0.3}$-LDH-1 performed much better than $MgAlCo_{0.3}$-LDH, indicating that Co^{3+} species might be the active sites in the reaction. However, the selectivity towards 1,2-epoxyhexane decreased obviously over these two catalysts. Only the embedment of trivalent Fe led to big enhancement of catalysis of the catalyst. The conversion of 1-hexene reached 90% with a 1,2-epoxyhexane selectivity of 99% over the trivalent Fe embedded catalyst $MgAlFe_{0.3}$-LDH. The catalytic performances on the epoxidation of the metal embedded MgAl-LDH were very similar to their catalysis in Baeyer–Villiger oxidation of ketones [20, 32]. It was revealed that the Fe^{3+} species are mainly octahedrally coordinated and formed cluster-type structure containing Fe^{3+}–O–Fe^{3+} species on the surface Mg–Al mixed oxides, working as the active sites for the oxidation of benzaldehyde to peroxybenzoic acid [20]. The peroxybenzoic acid generated in situ then oxidizes olefin such as 1-hexene to the epoxide. From the above results a general trend was concluded that the trivalent metal embedded catalyst showed high activity compared to its bivalent counterpart. In addition, the trivalent Fe embedded catalyst $MgAlFe_{0.3}$-LDH showed best performance among all the catalysts.

Since the catalyst $MgAlFe_{0.3}$-LDH showed best among the catalysts embedded with different metals in the epoxidation of 1-hexene with O_2/benzaldehyde, several $MgAlFe_x$-LDH catalysts embedded with different amount of Fe (x = 0.1, 0.2, 0.4 and 0.5) were prepared and evaluated in the same reaction to further improve the catalytic epoxidation reaction.

As shown in Table 3, the conversion of 1-hexene increased with increase in Fe content in the catalysts initially and reached its maximum of 97% at Fe content of 0.4, and decreased to 88% with further increase in Fe content to 0.5. The selectivity towards 1,2-epoxyhexane almost kept constant with the variation of Fe content in all the cases. As mentioned previously, the Fe^{3+} species on the catalyst surface are the active sites for the aerobic oxidation of benzaldehyde to peroxybenzoic acid, higher Fe content means more active sites in the catalyst, thus promoting the reaction. Therefore, the quantity and dispersion of Fe^{3+} species are more likely the key factors to influence the catalysis of the catalysts.

Table 3 Epoxidation of 1-hexene catalyzed by different $MgAlFe_x$-LDH

Entry	Catalyst	Conv. (%)	Sel. (%)
1	$MgAlFe_{0.1}$-LDH	29	99
2	$MgAlFe_{0.2}$-LDH	85	98
3	$MgAlFe_{0.3}$-LDH	90	99
4	$MgAlFe_{0.4}$-LDH	97	98
5	$MgAlFe_{0.5}$-LDH	88	99

Reaction conditions: 1-hexene 8 mmol, benzaldehyde 24 mmol, catalyst 0.05 g, solvent 1,2-dichloroethane 40 mL, O_2 10 mL/min, temperature 40 ℃, induction time 3 h, reaction time 2.5 h

3.3 Optimization of Reaction Conditions

With the excellent catalyst $MgAlFe_{0.4}$-LDH in hand, the parameters affecting the reaction including solvent and its volume, induction time, benzaldehyde dosage, reaction temperature, catalyst loading amount were screened to improve further the epoxidation of 1-hexene over the catalyst. Table 4 exhibits the effect of solvent on the reaction. As shown in the table, no reaction was detected in alcohols such as methanol, ethanol and isopropanol. The reaction also failed in toluene and dichloromethane. Only a moderate conversion of 1-hexene with a 1,2-epoxyhexane selectivity of 99% was obtained in acetonitrile. Gratifyingly, the reaction proceeded very well in 1,2-dichloroethane, and a conversion of 1-hexene as high as 97% with a selectivity of 99% towards 1,2-epoxyhexane was received. Generally, 1,2-dichloroethane (DCE) is also the best solvent in Baeyer–Villiger oxidation with O_2/benzaldehyde over various catalysts [32, 47, 48], no answer is available for its excellent performance in the related reactions.

It was found that the induction time, which is the preoxidation period before addition of 1-hexene, had significant effect on the epoxidation reaction. As shown in Fig. 6, both the conversion of 1-hexene and the selectivity of 1,2-epoxyhexane increased with the extension of induction time initially. When the induction time was extended to 2.5 h, the conversion of 1-hexene increased to 96%, and the selectivity

Table 4 The effect of solvent on the reaction

Entry	Solvent	Conv. (%)	Sel. (%)
1	1,2-dichloroethane	97	99
2	Methanol	–	–
3	Ethanol	–	–
4	Isopropanol	–	–
5	Toluene	–	–
6	Acetonitrile	74	99
7[a]	Dichloromethane	5	91

Reaction conditions: 1-hexene 8 mmol, benzaldehyde 24 mmol, $MgAlFe_{0.4}$-LDH 0.05 g, solvent 40 mL, O_2 10 mL/min, temperature 40 ℃, induction time 3 h, reaction time 2.5 h

[a]Temperature 25 ℃

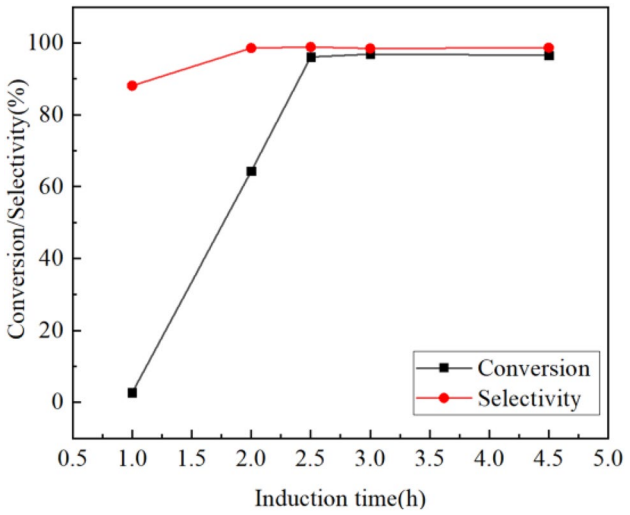

Fig. 6 The effect of induction time on the reaction. Reaction conditions: 1-hexene 8 mmol, benzaldehyde 24 mmol, $MgAlFe_{0.4}$-LDH 0.05 g, DCE 40 mL, O_2 10 mL/min, temperature 40 ℃, reaction time 2.5 h

of 1,2-epoxyhexane reached 99%. Then both of them maintained almost constant with further extending induction time. It was assumed that the epoxidation reaction with O_2/benzaldehyde via two steps: catalytic aerobic oxidation of benzaldehyde to peroxybenzoic acid; epoxidation of 1-hexene by peroxybenzoic acid generated in situ. However, the epoxidation reaction could only proceed when enough peroxyacid was formed, which needed a period of time, being the induction time.

The amount of benzaldehyde is an important factor influencing the epoxidation of 1-hexene with O_2/benzaldehyde. As shown in Fig. 7, the conversion of 1-hexene increased with increase in benzaldehyde amount initially, and reached 96% with a selectivity towards 1,2-epoxyhexane of 99% at benzaldehyde to 1-hexene molar ratio of 3:1, then maintained constant with a further increase in benzaldehyde amount. Meanwhile, the selectivity towards 1,2-epoxyhexane changed slightly with the benzaldehyde amount.

The effect of reaction temperature on the epoxidation of 1-hexene was also investigated. As shown in Fig. 8, the conversion of 1-hexene was very low at 35 °C, but increased significantly to 96% with reaction temperature increased to 40 °C, then gently increased to its maximum of 99% with a 1,2-epoxyhexane selectivity of 99% at 45 °C. With a further increase in reaction temperature, the conversion of 1-hexene decreased obviously, which might be due to the decomposition of peroxybenzoic acid at higher temperature. Therefore, the optimal temperature of the reaction is 45 ℃. It was found that the selectivity of 1,2-epoxyhexane almost kept constant at all the reaction temperatures.

As shown in Fig. 9, the amount of DCE had big influence on the reaction. The conversion of 1-hexene was very small at low DCE loading, and increased with the amount of DCE. When the amount of DCE increased to 25 mL, the conversion of 1-hexene increased to 98% with a 1,2-epoxyhexane selectivity of 98%. Then both the conversion of 1-hexene and the selectivity of 1,2-epoxyhexane increased slightly with a further increase in DCE loading. The results indicated the importance of DCE in the catalytic aerobic oxidation of benzaldehyde to peroxybenzoic acid, thus affecting the epoxidation reaction.

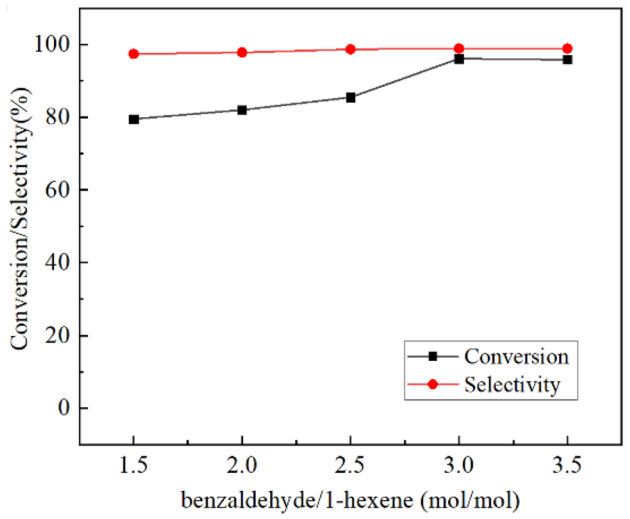

Fig. 7 The effect of benzaldehyde amount on the reaction. Reaction conditions: 1-hexene 8 mmol, $MgAlFe_{0.4}$-LDH 0.05 g, DCE 40 mL, O_2 10 mL/min, induction time 2.5 h, reaction time 2.5 h, temperature 40 ℃

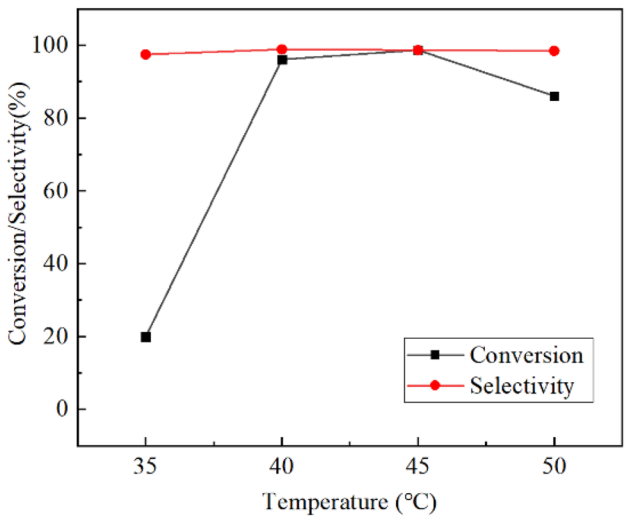

Fig. 8 The effect of temperature on the reaction. Reaction conditions: 1-hexene 8 mmol, benzaldehyde 24 mmol, $MgAlFe_{0.4}$-LDH 0.05 g, DCE 40 mL, O_2 10 mL/min, induction time 2.5 h, reaction time 2.5 h

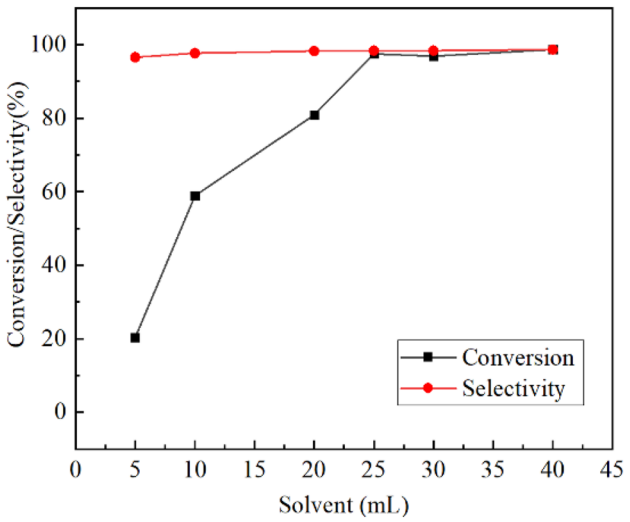

Fig. 9 The effect of solvent amount on the reaction. Reaction conditions: 1-hexene 8 mmol, benzaldehyde 24 mmol, $MgAlFe_{0.4}$-LDH 0.05 g, O_2 10 mL/min, temperature 45°C, induction time 2.5 h, reaction time 2.5 h

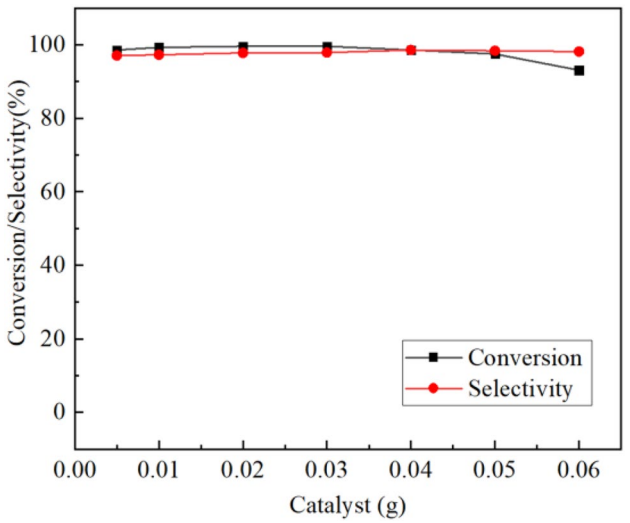

Fig. 10 The effect of $MgAlFe_{0.4}$-LDH amount on the reaction. Reaction conditions: 1-hexene 8 mmol, benzaldehyde 24 mmol, O_2 10 mL/min, DCE 25 mL, temperature 45 ℃, induction time 2.5 h, reaction time 2.5 h

The amount of catalyst dosage in the reaction was also screened and it was found as shown in Fig. 10 that the catalyst dosage had no significant influence on the reaction in the screen range of 0.005 to 0.05 g. The conversion of 1-hexene was always close to 99% with 1,2-epoxyhexane of 97%.

Based on the experimental results and in view of the minimization of solvent and catalyst dosages, the optimal parameters were determined to be 1-hexene 8 mmol, benzaldehyde 24 mmol, catalyst dosage 0.005 g, DCE 25 mL, O_2 10 mL/min, reaction temperature 45 °C, induction time 2.5 h, and reaction time 2.5 h. Under these conditions, the conversion of 1-hexene was 99% with 1,2-epoxyhexane of 97%.

3.4 Hot Filtration and Recycle Tests

In order to illustrate the stability of the catalyst and the heterogeneity of the reaction, a hot filtration experiment was carried out. Because the epoxidation of olefin with benzaldehyde/O_2 proceeds in two elementary steps: the catalytic oxidation of benzaldehyde with O_2 to peroxybenzoic acid, and the non-catalytic epoxidation of olefin with peroxybenzoic acid to epoxide, the catalyst was filtered out after induction time of 0.5 h. As shown in Fig. 11, the amount of peroxybenzoic acid changed slightly with induction time under O_2 bubbling after the catalyst was removed. In addition, 1-hexene was injected into the filtrate at induction time of 2.5 h to run the epoxidation reaction as that in the presence of catalyst. The conversion of 1-hexene was only half of that in the presence of catalyst at the same reaction time of 1 h, then maintained constant with extending reaction time, which could be ascribed to no peroxybenzoic acid was generated in the absence of catalyst to support further epoxidation of 1-hexene. The results indicated that the epoxidation of olefin with benzaldehyde/O_2 over the catalyst $MgAlFe_{0.4}$-LDH belongs to a heterogeneous catalytic process, no obvious leaching of Fe took place during the reaction which was confirmed by ICP analysis. The ICP analysis revealed that the Fe contents of the fresh and used catalyst samples are 4.69% and 4.67%, respectively.

After catalytic run, the catalyst $MgAlFe_{0.4}$-LDH was recovered by filtration, washing with DCE and drying, and then subjected to the next run under the same reactions. As shown in Fig. 12, the conversion of 1-hexene changed slightly and maintained above 97% in the first five runs. In the sixth run, the conversion of 1-hexene decreased to 93%. In all the cases, the selectivity of 1,2-epoxyhexane maintained constant. The results indicated that the catalyst has good stability and recyclability.

3.5 Substrate Scope

Finally, the catalyst $MgAlFe_{0.4}$-LDH was applied to the epoxidation of different olefins to evaluate its substrate applicability under the optimized conditions. As can be seen from Table 5, all the olefins, including terminal aliphatic olefines, cyclohexene and styrene, were converted to the corresponding epoxides in high conversion and selectivity, indicating its broad substrate scope of catalyst $MgAlFe_{0.4}$-LDH.

The catalyst $MgAlFe_{0.4}$-LDH was compared with some LDH based catalysts in literature. As shown in Table 6, the catalyst $MgAlFe_{0.4}$-LDH showed the best performance in the epoxidation of 1-octene using O_2 or H_2O_2 as terminal

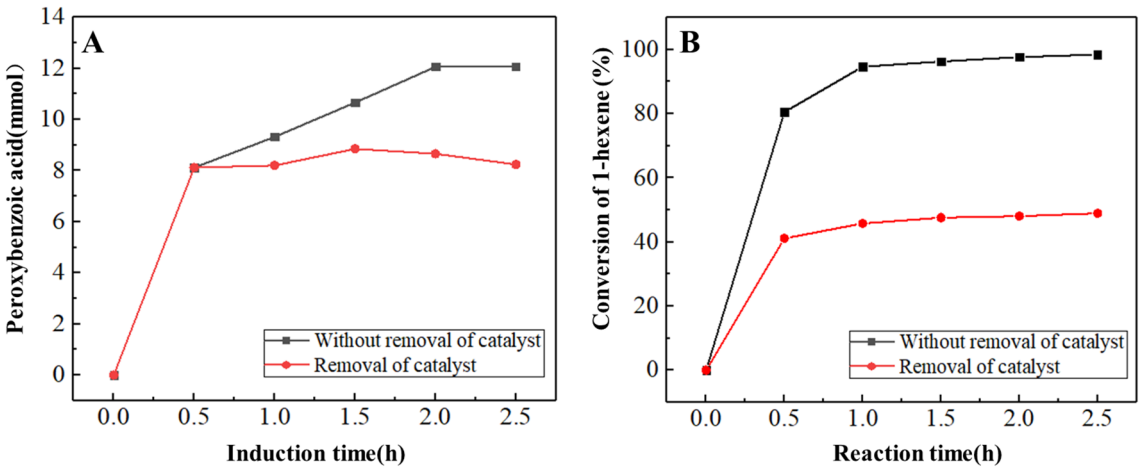

Fig. 11 Hot filtration test of $MgAlFe_{0.4}$-LDH. Reaction conditions: olefin 8 mmol, benzaldehyde 24 mmol, O_2 10 mL/min, DCE 25 mL, $MgAlFe_{0.4}$-LDH 0.005 g, temperature 45 °C, induction time 2.5 h, reaction time 2.5 h

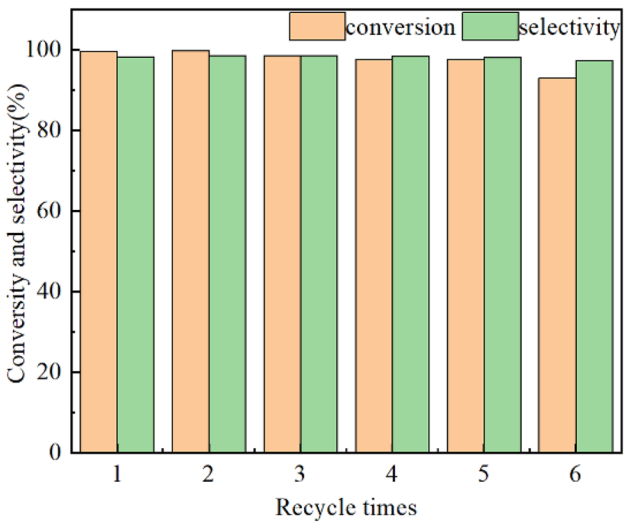

Fig. 12 Recycle test of $MgAlFe_{0.4}$-LDH

Table 5 The epoxidation of other alkenes catalyzed by $MgAlFe_{0.4}$-LDH

Entry	Substrate	Conv. (%)	Sel. (%)
1	1-pentene	100	96
2	1-hexene	99	97
3	1-octene	98	98
4	1-decene	98	98
5	cyclohexene	100	95
6	styrene	100	95

Reaction conditions: olefin 8 mmol, benzaldehyde 24 mmol, O_2 10 mL/min, DCE 25 mL, $MgAlFe_{0.4}$-LDH 0.005 g, temperature 45 ℃, induction time 2.5 h, reaction time 2.5 h

oxidant in view of both epoxide yield and mild reaction conditions. The results indicated that the embedment of Fe^{3+} species in MgAl-LDH enhanced the catalysis of MgAl-LDH in the epoxidation, and the embedded Fe^{3+} species are more active than their Co^{3+} counterparts.

4 Conclusion

Several MgAl-LDH based catalysts embedded with Ni, Cu, Fe, Zn, Co and Mn were synthesized by co-precipitation method. The characterization results revealed that these catalysts had hydrotalcite-like structures with interlayer anions CO_3^{2-}. For the Fe embedded catalysts $MgAlFe_x$-LDH, the Fe are fully incorporated into the Mg/Al-LDH layers in the state of Fe^{3+}, and are mainly octahedrally coordinated and formed cluster-type structure containing Fe^{3+}–O–Fe^{3+} species on the surface Mg–Al mixed oxides, working as the active sites for the oxidation of benzaldehyde to peroxybenzoic acid, endowing the catalysts $MgAlFe_x$-LDH especially $MgAlFe_{0.4}$-LDH excellent catalytic activity and selectivity in the epoxidation of various olefins with O_2/benzaldehyde under mild conditions. The catalyst $MgAlFe_{0.4}$-LDH also has good stability and recyclability, and broad substrate applicability.

Table 6 Comparison of $MgAlFe_{0.4}$-LDH with other catalysts in the epoxidation of 1-octene

Entry	Substrate	Catalyst	Time (h)	Yield (%)	References
1[a]	1-octene	$Mg_{10}Al_2(OH)_{24}CO_3$	24	80	[49]
2[b]	1-octene	$Mg_{10}Al_2(OH)_{24}CO_3$	24	95	[50]
3[c]	1-octene	CoTPPS/NiAl-$LDH_{3.0}$	6	89	[30]
4[d]	1-octene	CoPcTs-Zn_2Al-LDH	4	85	[29]
5[e]	1-octene	Co_2Al–LDH	7	78	[51]
6[f]	1-octene	$MgAlFe_{0.4}$-LDH	5	96	This work

Reaction conditions:

[a]Substrate 4 mmol, isobutyramide 40 mmol, $Mg_{10}Al_2(OH)_{24}CO_3$ (0.15 g), 1,2-dichloroethane 10 mL, 30% aq. H_2O_2 4.5 mL, 48 mmol, sodium dodecyl sulfate 0.2 mmol, 70 °C

[b]Substrate 3.9 mmol, $Mg_{10}Al_2(OH)_{24}CO_3$ 0.05 g, PhCN 10.5 mmol, MeOH (10 ml), 30% aq. H_2O_2 (2.4 ml), 60 °C

[c]Substrate 2 mmol, isobutyraldehyde 6 mmol, CoTPPS/NiAl-$LDH_{3.0}$ 0.002 mmol, CH_3CN 4 mL, O_2 bubbling, 40 °C

[d]Substrate 2 mmol, CoPcTs-Zn_2Al-LDH 6 mg, acetonitrile 8 mL, IBA 5 mmol, O_2 15 mL/min, 60 °C

[e]Substrate 1 mmol, Co_2Al–LDH 50 mg, acetonitrile 2 mL, IBA 3 mmol, O_2 25 mL/min,60 °C

[f]Substrate 8 mmol, benzaldehyde 24 mmol, O_2 10 mL/min, DCE 25 mL, $MgAlFe_{0.4}$-LDH 0.005 g, 45 ℃

Acknowledgements Financial supports were received from the National Natural Science Foundation of China (Grant No. 21776056), and the Foundation of Central Government Guides Local Science and Technology Development (Grant Nos. 206Z4001G, 216Z1401G).

Declarations

Conflict of interest The authors declare that they have no conflict of interest.

References

1. Mizuno N, Yamaguchi K, Kamata K (2005) Epoxidation of olefins with hydrogen peroxide catalyzed by polyoxometalates. Coord Chem Rev 249(17–18):1944–1956
2. Yang B, Storey RF (2020) Synthesis and characterization of polyisobutylene telechelic prepolymers with epoxide functionality. React Funct Polym 150:104563
3. Gomes AR, Varela CL, Tavares-da-Silva EJ, Roleira FMF (2020) Epoxide containing molecules: A good or a bad drug design approach. Eur J Med Chem 201:112327
4. Das A, Bhaumik A, Pathak T (2020) Epoxides of D-fructose and L-sorbose: A convenient class of "click" functionality for the synthesis of a rare family of amino- and thio-sugars. Carbohydr Res 487:107870
5. Jørgensen KA (1989) Transition-metal-catalyzed epoxidations. Chem Rev 89:431–458
6. Shen J, Ye SC, Xu XY, Liang JX, He GY, Chen H (2019) Reduced graphene oxide based NiCo layered double hydroxide nanocomposites: An efficient catalyst for epoxidation of styrene. Inorg Chem Commun 104:219–222
7. Teran J, Huš M, Likozar B, Djinović P (2020) Propylene epoxidation using molecular oxygen over copper-and silver-based catalysts: A review. ACS Catal 10(22):13415–13436
8. Grigoropoulou G, Clark JH, Elings JA (2002) Recent developments on the epoxidation of alkenes using hydrogen peroxide as an oxidant. Green Chem 5:1–7
9. Batra MS, Dwivedi R, Prasad R (2019) Recent developments in heterogeneous catalyzed epoxidation of styrene to styrene oxide. Chemistry Select 4(40):11636–11673
10. Sharma AS, Sharma VS, Kaur H, Varma RS (2020) Supported heterogeneous nanocatalysts in sustainable, selective and eco-friendly epoxidation of olefins. Green Chem 22(18):5902–5936
11. Jiang J, Ma K, Zheng YF, Cai SL, Li R, Ma J (2009) Cobalt salophen complex immobilized into montmorillonite as catalyst for the epoxidation of cyclohexene by air. Appl Clay Sci 45(3):117–122
12. Tian S, Peng C, Dong J et al (2021) High-loading single-atomic-site silver catalysts with an Ag_1–C_2N_1 structure showing superior performance for epoxidation of styrene. ACS Catal 11(9):4946–4954
13. Punniyamurthy T, Velusamy S, Iqbal J (2005) Recent advances in transition metal catalyzed oxidation of organic substrates with molecular oxygen. Chem Rev 105(6):2329–2363
14. Turner M, Golovko VB, Vaughan OP et al (2008) Selective oxidation with dioxygen by gold nanoparticle catalysts derived from 55-atom clusters. Nature 454(7207):981–983
15. Wang QX, Zhan C, Zhou LY, Fu G, Xie ZX (2019) Effects of Cl^- on Cu_2O nanocubes for direct epoxidation of propylene by molecular oxygen. Catal Commun 135:105897
16. Hassan S, Kumar R, Tiwari A et al (2018) Role of oxygen vacancy in cobalt doped ceria catalyst for styrene epoxidation using molecular oxygen. Mol Catal 451:238–246
17. Brown JW, Nguyen QT, Otto T, Jarenwattananon NN, Glöggler S, Bouchard L-S (2015) Epoxidation of alkenes with molecular oxygen catalyzed by a manganese porphyrin-based metal–organic framework. Catal Commun 59:50–54
18. Teržan J, Huš M, Likozar B, Djinović P (2020) Propylene epoxidation using molecular oxygen over copper- and silver-based catalysts: a review. ACS Catal 10:1013415
19. Monnier JR (2001) The direct epoxidation of higher olefins using molecular oxygen. Appl Catal A-Gen 221(1):73–91
20. Kawabata T, Fujisaki N, Shishido T, Nomura K, Sano T, Takehira K (2006) Improved Fe/Mg-Al hydrotalcite catalyst for Baeyer-Villiger oxidation of ketones with molecular oxygen and benzaldehyde. J Mol Catal A: Chem 253(1–2):279–289
21. Mallakpour S, Hatami M, Hussain CM (2020) Recent innovations in functionalized layered double hydroxides: Fabrication,

characterization, and industrial applications. Adv Colloid Interface Sci 283:102216
22. Rives V, del Arco M, Martín C (2014) Intercalation of drugs in layered double hydroxides and their controlled release: A review. Appl Clay Sci 88–89:239–269
23. San Román MS, Holgado MJ, Salinas B, Rives V (2013) Drug release from layered double hydroxides and from their polylactic acid (PLA) nanocomposites. Appl Clay Sci 71:1–7
24. Abdollahzadeh M, Hosseini E, Ahmadi H et al (2021) Low humid transport of anions in layered double hydroxides membranes using polydopamine coating. J Membr Sci 624:118974
25. Dewangan N, Hui WM, Jayaprakash S et al (2020) Recent progress on layered double hydroxide (LDH) derived metal-based catalysts for CO_2 conversion to valuable chemicals. Catal Today 356:490–513
26. Yan K, Liu YQ, Lu YR, Chai JJ, Sun LP (2017) Catalytic application of layered double hydroxide-derived catalysts for the conversion of biomass-derived molecules. Catal Sci Technol 7:1622–1645
27. Fan G, Li F, Evans DG, Duan X (2014) Catalytic applications of layered double hydroxides: Recent advances and perspectives. Chem Soc Rev 43(20):7040–7066
28. Guo J, Jiao QZ, Shen JP, Jiang DZ (1996) Catalytic oxidation of cyclohexene with molecular oxygen by polyoxometalate-intercalated hydrotalcites. Catal Lett 40:43–45
29. Zhou W, Zhou J, Chen Y et al (2017) Metallophthalocyanine intercalated layered double hydroxides as an efficient catalyst for the selective epoxidation of olefin with oxygen. Appl Catal A: Gen 542:191–200
30. Shen C, Ma J, Zhang T et al (2020) Intercalated cobalt porphyrin between layered double hydroxide nanosheets as an efficient and recyclable catalyst for aerobic epoxidation of alkenes. Appl Clay Sci 187:105478
31. Wang X, Liang Z, Zhang F, Yang L, Xu S (2013) Enhanced catalytic performances of Ag nanoparticles supported on layered double hydroxide for styrene epoxidation. J Mater Sci 48(17):5899–5903
32. Kaneda K, Ueno S, Imanaka T (1995) Catalysis of transition metal-functionalized hydrotalcites for the Baeyer-Villiger oxidation of ketones in the presence of molecular oxygen and benzaldehyde. J Mol Catal A: Chem 102:135–138
33. Xu Z, Zeng H (2000) In-situ generation of maximum trivalent cobalt in synthesis of hydrotalcite-like compounds $Mg_xCo^{II}_{1-x-y}Co^{III}_y(OH)_2(NO_3)_y{\cdot}nH_2O$. Chem Mater 12:2597–2603
34. Zhao Y, Li F, Zhang R, Evans DG, Duan X (2002) Preparation of layered double-hydroxide nanomaterials with a uniform crystallite size using a new method involving separate nucleation and aging steps. Chem Mater 14(10):4286–4291
35. Ahmed IM, Gasser MS (2012) Adsorption study of anionic reactive dye from aqueous solution to Mg–Fe–CO_3 layered double hydroxide (LDH). Appl Surf Sci 259:650–656
36. Gao J, Tong X, Li X, Miao H, Xu J (2007) The efficient liquid-phase oxidation of aromatic hydrocarbons by molecular oxygen in the presence of $MnCO_3$. J Chem Technol Biotechnol 82(7):620–625
37. Wang H, Jing M, Wu Y, Chen W, Ran Y (2018) Effective degradation of phenol via fenton reaction over CuNiFe layered double hydroxides. J Hazard Mater 353:53–61
38. Fernandez JM, Ulibarri MA, Labajosb FM, Rives V (1998) The effect of iron on the crystalline phases formed upon thermal decomposition of Mg-Al-Fe hydrotalcites. J Mater Chem A 8:2507–2514
39. Dávila V, Lima E, Bulbulian S, Bosch P (2008) Mixed Mg(Al)O oxides synthesized by the combustion method and their recrystallization to hydrotalcites. Microporous Mesoporous Mater 107(3):240–246
40. Trujillano R, Holgado MJ, González JL, Rives V (2005) Cu-Al-Fe layered double hydroxides with CO_3^{2-} and anionic surfactants with different alkyl chains in the interlayer. Solid State Sci 7(8):931–935
41. Antonyraj CA, Kannan S (2011) Influence of co-bivalent ions in Cu-containing LDHs and solvent on hydroxylation of benzene to phenol. Appl Clay Sci 53(2):297–304
42. Li S-S, Jiang M, Jiang T-J, Liu J-H, Guo Z, Huang X-J (2017) Competitive adsorption behavior toward metal ions on nano-Fe/Mg/Ni ternary layered double hydroxide proved by XPS: Evidence of selective and sensitive detection of Pb(II). J Hazard Mater 338:1–10
43. Yamashita T, Hayes P (2008) Analysis of XPS spectra of Fe^{2+} and Fe^{3+} ions in oxide materials. Appl Surf Sci 254(8):2441–2449
44. Gong C, Chen F, Yang Q et al (2017) Heterogeneous activation of peroxymonosulfate by Fe-Co layered doubled hydroxide for efficient catalytic degradation of Rhoadmine B. Chem Eng J 321:222–232
45. Ma J, Yang M, Chen Q et al (2017) Comparative study of Keggin-type polyoxometalate pillared layered double hydroxides via two synthetic routes: Characterization and catalytic behavior in green epoxidation of cyclohexene. Appl Clay Sci 150:210–216
46. Zhao J, Chen J, Xu S et al (2014) Hierarchical NiMn layered double hydroxide/carbon nanotubes achitecture with superb energy density for flexible supercapacitors. Adv Funct Mater 2(20):2938–2946
47. Liu G, Sun L, Luo W et al (2018) Aerobic Baeyer-Villiger oxidation of ketones over mesoporous Mn-Ce and Mn-Co composite oxides in the presence of benzaldehyde: the Effect of valence state. Mol Catal 458:9–18
48. Nabae Y, Rokubuichi H, Mikuni M, Kuang Y, Hayakawa T (2013) Catalysis by carbon materials for the aerobic Baeyer-Villiger oxidation in the presence of aldehydes. ACS Catal 3(2):230–236
49. Yamaguchi K, Ebitani K, Kaneda K (1999) Hydrotalcite-catalyzed epoxidation of olefins using hydrogen peroxide and amide compounds. J Org Chem 64:2966–2968
50. Kaneda K, Yamaguchi K, Mori K, Mizugaki T, Ebitani K (2000) Catalyst design of hydrotalcite compounds for efficient oxidations. Catal Surv Jpn 4(1):31–38
51. Dai X, Huang J, Tang S, Zheng X, Peng X (2020) Efficient aerobic epoxidation of olefins accelerated by a bifunctional Co_2Al layered double hydroxide. React Kinet Mech Cat 131(1):1–14